Atmospheric wind biases: A challenge for simulating the Arctic Ocean in coupled models?

C. Hinrichs[1], Q. Wang[1,2], N. Koldunov[1], L. Mu[3], T. Semmler[1], D. Sidorenko[1], and T. Jung[1]

[1] Alfred Wegener Institute Helmholtz Center for Polar and Marine Research.

[2] Laboratory for Regional Oceanography and Numerical Modeling, Pilot National Laboratory for Marine Science and Technology (Qingdao), Qingdao, China.

[3] Qingdao National Laboratory for Marine Science and Technology, Qingdao, China.

Corresponding author: Claudia Hinrichs (Claudia.Hinrichs@awi.de)

Key Points:

- Many state-of-the-art climate models do not simulate Atlantic Water in the Arctic Ocean realistically enough.
- Biases in sea level pressure and wind in coupled models can interrupt and reverse Atlantic Water circulation at intermediate depth.
- Underestimation of sea ice cover can amplify this problem further.

Abstract

Many state-of-the-art climate models do not simulate the Atlantic Water (AW) layer in the Arctic Ocean realistically enough to address the question of future Arctic Atlantification and its associated feedback. Biases concerning the AW layer are commonly related to insufficient resolution and exaggerated mixing in the ocean component as well as unrealistic Atlantic-Arctic Ocean exchange. Based on sensitivity experiments with FESOM1.4, the ocean-sea ice component of the global climate model AWI-CM1, we show that even if all impediments for simulating AW realistically are addressed in the ocean model, new biases in the AW layer develop after coupling to an atmosphere model. By replacing the wind forcing over the Arctic with winds from a coupled simulation we show that a common bias in the atmospheric sea level pressure (SLP) gradient and its associated wind bias lead to differences in surface stress and Ekman transport. Fresh surface water gets redistributed leading to changes in steric height distribution. Those changes lead to a strengthening of the anticyclonic surface circulation in the Canadian Basin, so that the deep counterflow carrying warm AW gets reversed and a warm bias in the Canadian Basin develops. An underestimation of sea ice concentration can significantly amplify the induced ocean biases. The SLP and anticyclonic wind bias in the Nordic Seas weaken the cyclonic circulation leading to reduced AW transport into the Arctic Ocean through Fram Strait but increased AW transport through the Barents Sea Opening. These effects together lead to a cold bias in the Eurasian Basin.

Plain Language Summary

Coupled global climate models are used to predict anthropogenic climate change along with its impacts. The Arctic has experienced amplified warming in the recent decades compared to global mean warming and therefore is one region of intense climate research. In this context Atlantification of the Arctic has become a high priority topic. Atlantification, describes the increasing impact of oceanic heat in the form of Atlantic-origin water within the Arctic Ocean and on the sea ice cover. In climate models, the direction and strength of simulated Atlantic Water (AW) circulation around the Arctic Ocean is known to be sensitive to ocean grid resolution, parametrization, boundary and surface forcing or a combination thereof. Here we show that biases in the atmospheric component of climate models can interrupt and even reverse

the simulated AW circulation at depth. Such biases can be further amplified by negative bias in simulated sea ice. The impact pathways of the wind biases are investigated in this study.

1 Introduction

The Arctic is one of the fastest changing regions in the world (Serreze et al. 2009; Serreze and Barry 2011) and hence has attracted an increasing amount of scientific work. Global climate models are used to predict changes in the climate system, including the Arctic, that may occur in a warming world and to understand climate dynamics and associated feedback. There is an ongoing effort to improve the representation of key processes in contemporary climate models in general and in the Arctic specifically, with the ultimate aim to increase predictive capacity (Jung et al. 2016). One of the processes of particular interest is the oceanic heat transport from the North Atlantic into the Arctic Ocean in the form of Atlantic Water (AW) inflow and the subsequent AW circulation and heat distribution within the Arctic Basin and how it will change in the future.

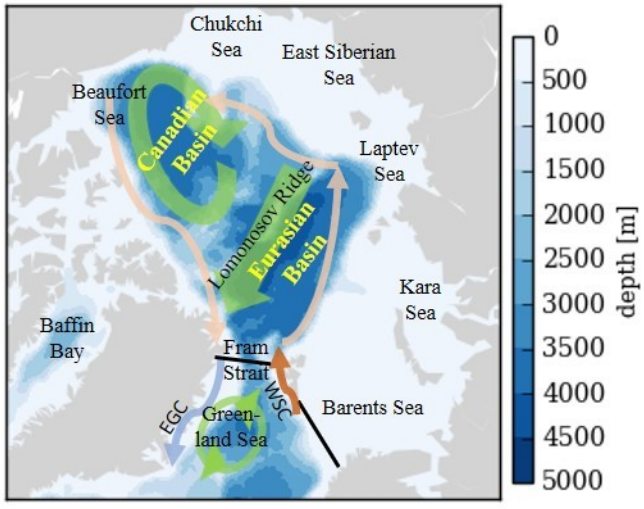

Figure 1. Map of the Arctic Ocean. The two main basins (Canadian and Eurasian Basin) divided by the Lomonosov Ridge, the shelf seas and neighboring seas are depicted. A schematic view of the dominant features of the Arctic Ocean circulation shows the anticyclonic Beaufort Gyre System, the Transpolar Drift System in green and the subsurface cyclonic flow of AW around the Arctic Basin is sketched in pink. South of Fram Strait, the Greenland Sea Gyre (GSG) is sketched in green, and the West Spitsbergen Current (WSP, orange) and the East Greenland Current (EGC, lightblue) are shown. Sections where transports through Fram Strait and the southern Barents Sea Opening are computed are shown in black.

Over the last few decades, a warming trend in the AW layer has been observed at Fram Strait and in the Arctic Ocean (Polyakov et al. 2005; Dmitrenko et al. 2008; Beszczynska-Möller et al. 2012; Polyakov et al. 2013). This warming trend of the AW layer together with weaker

stratification in the upper ocean has been termed *Atlantification* by Polyakov et al. (2017). This phenomenon has been identified as critical in a warming Arctic. In the Barents Sea, Atlantification leads to increased bottom melt of sea ice, more open water area, increased surface temperatures and lower albedo (Koenigk and Brodeau 2014; Barton et al. 2018). In the Eurasian Basin (EB), Atlantification is associated with weakened stratification, increased vertical mixing, and increased sea-ice decline (Polyakov et al. 2017; Ivanov et al. 2018; Polyakov et al. 2020). The sea ice decrease, caused by Atlantification and its associated feedback, contributes to amplified climate change in the Arctic. Sea ice decline also affects the AW layer in the Arctic Ocean. A model study by (Itkin et al. 2014), for example, suggests that thinner, more mobile sea ice in the central Arctic weakens the cyclonic circulation of AW. Another study by Wang et al. (2020) shows that the Arctic sea ice decline has strengthened the AW heat influx through Fram Strait by impacting the ocean circulation in the Nordic Seas. There is also an ongoing debate that Arctic changes, and especially sea ice cover in the Barents Sea, could possibly have a large influence on the lower latitude ocean and climate (e.g. Vihma 2014; Wallace et al. 2014; Cohen et al. 2020).

In order to understand and predict the evolution of this complex system coupled climate models constrained by observations are an important tool. However, the degree to which we can trust climate model predictions of the future role of Atlantification in Arctic climate change, hinges on their ability to simulate the present-day AW inflow and circulation within the Arctic Ocean realistically.

The circulation of the Arctic Ocean can be described as a two-layer system (e.g. Aagaard 1989; for a recent, comprehensive review of Arctic Ocean circulation dynamics see Timmermans and Marshall 2020). The large-scale ocean surface circulation is anticyclonic, driven by the dominating wind systems centered over the Beaufort Gyre and the Transpolar Drift Zone. Below the surface layer the flow at intermediate depth is largely concentrated in narrow boundary currents along the steep slopes of the Eurasian and Canadian Basins (see Figure 1). These boundary currents flow in cyclonic direction around the deep Arctic Basin, opposite to the upper ocean drift. Relatively warm and salty AW circulates the Arctic in this cyclonic boundary current (Rudels et al. 1999; Woodgate et al. 2001; Karcher et al. 2007; Spall 2013) at a mean depth of around 400m. The strength and direction of this Arctic circumpolar boundary current (ACBC)

101 determines the spatial distribution and storage of heat in the Arctic Ocean at this intermediate
102 depth.

103 With this in mind, we compared the 400 m temperature layer in the Alfred Wegener
104 Institute coupled climate model AWI-CM1 (Sidorenko et al. 2015; Rackow et al. 2016; Semmler
105 et al. 2020) to the PHC3.0 climatology (Steele et al. 2001) (Figure 2). The horizontal temperature
106 distribution can serve as a proxy for AW circulation in the Arctic Ocean. For the AWI-CM1
107 simulation, the comparison reveals an unrealistic distribution of AW: Warm AW that enters
108 through Fram Strait does not follow the Arctic's deep basin slope cyclonically; it rather gets
109 diverted westward towards the Canadian Basin. The result is a cold bias in the eastern Eurasian
110 Basin and a warm bias in the Canadian Basin that is reminiscent of an anticyclonic circulation
111 pattern.

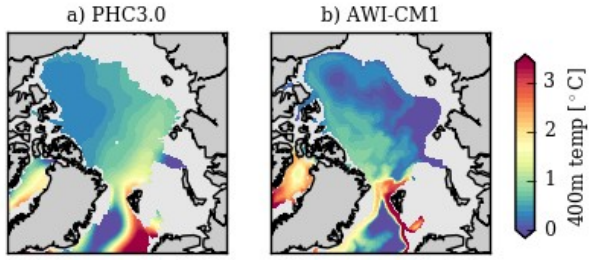

112

113 **Figure 2**. 400 m temperature from PHC3.0 climatology (a) and a 10-year average from a coupled AWI-CM1.1
114 simulation (b). Shown here is a simulation on an ocean grid with 25km resolution north of 50°N and T63
115 atmospheric resolution. A similar bias pattern is also evident in runs with higher ocean or atmosphere resolution.

116 This finding came somewhat as a surprise, after standalone simulations with AWI-CM1's
117 ocean-sea ice component FESOM1.4 had shown a very realistic temperature distribution and a
118 cyclonic circumpolar boundary current for horizontal resolutions of 25 km and 4.5 km in Arctic
119 (Wang et al. 2018).

120 It is worth stressing that not only AWI-CM1 is deficient in simulating the propagation of
121 AW around the Arctic, as revealed by some recent studies. Shu et al. (2019), for example,
122 evaluated a number of CMIP5 models and found that 9 out of 41 participating models did not
123 simulate a well-defined AW layer at all. The multi-model mean (MMM) AW layer derived from
124 the other 32 models was too thick and too deep. Furthermore, they found that the interannual
125 variability in AW temperature was much weaker than observed; and none of the models
126 simulated the observed warming trend of the recent decades. A follow-up study of 23 CMIP6
127 models by (Khosravi et al., submitted) shows that the AW layer is still too deep and too thick in

most models and the MMM, thus suggesting that the representation of the Arctic Ocean hydrography did not visibly improve from CMIP5 to CMIP6. Preceding CMIP6, the problem of incorrect AW simulation was also recognized in standalone ocean models in the CORE-II model intercomparison study (Ilıcak et al. 2016). Suggested solutions for the AW problem have been focusing on improving the ocean-sea ice model and include moving to higher-order advections schemes (Maqueda and Holloway 2006; Holloway et al. 2007), using eddy–topography interaction parameterization ("Neptune parametrization") (e.g. Golubeva and Platov 2007; Holloway and Wang 2009; Nazarenko et al. 1998), tuning vertical mixing (Zhang and Steele 2007) and increasing horizontal resolution (Wang et al. 2018). We find for AWI-CM1 that additional challenges can arise when a well-tuned (with respect to AW in the Arctic Ocean) ocean-sea ice model, here FESOM 1.4 (Wang et al. 2014; Danilov et al. 2015), is coupled to an atmospheric model, in this case ECHAM6.3 (Stevens et al. 2013), to form a coupled climate model.

In this paper we aim to understand the processes causing the deterioration of the AW layer in AWI-CM1. If the standalone version of an ocean-sea ice model can successfully replicate the two-layer circulation in the Arctic Ocean, but coupling leads to a perturbed AW circulation, then the reason must lie in the changes in ocean surface forcing after coupling with the atmosphere model. Our investigations narrowed the potential origins of these biases down to a large-scale bias in sea level pressure and the associated wind field and a negative bias in the sea ice cover in the coupled model, both have an impact on the surface stress imparted on the ocean. We conducted sensitivity experiments with our standalone ocean-sea ice model, to analyze the influence of biased wind and biased sea ice cover over the Arctic .

2 Model set-up and sensitivity experiments

2.1 FESOM1.4 Model Configuration

To study the effect of atmosphere forcing and sea ice concentration on the AW circulation we use the **F**inite **E**lement **S**ea ice-**O**cean **M**odel FESOM1.4 (Wang et al. 2014; Danilov et al. 2015) in standalone mode. FESOM1.4 is the ocean-sea ice component of the Alfred-Wegener-Institute's climate model version 1 (AWI-CM1) which is coupled to ECHAM6.3 (Stevens et al. 2013). The global performance of AWI-CM1 has been evaluated in Sidorenko et al. (2015) and Rackow et al. (2016), and for the AWI-CM1 CMIP6 contribution by Semmler et al. (2020).

FESOM employs unstructured grids which allow for increased grid resolution in an area of interest (e.g., the Arctic) while keeping the resolution coarser elsewhere. This, along with excellent scalability characteristics (Koldunov et al. 2019), makes longer, global simulations affordable. The problem with incorrect AW circulation and distribution in the coupled set-up is almost independent of ocean and atmosphere resolution (at least for AWI-CM1). Therefore, the sensitivity experiments are run on the 'baseline' ocean grid which was developed for the participation in the CORE-II Model Intercomparison Study (Griffies et al. 2009; Wang et al. 2016a, 2016b; Ilıcak et al. 2016). We will compare our sensitivity experiments to a coupled historical simulation run on the same ocean grid and an atmospheric resolution of T63 in the horizontal and 47 vertical levels. The ocean grid has a nominal resolution of 1° globally; however, the resolution has been refined to about 25 km north of 50°N and to 1/3° at the equator, and it is also refined moderately along the coasts. In the CORE-II model intercomparison study the ocean circulation itself is not evaluated, but the 400 m temperature layer is shown for each model, and for FESOM1.4 the temperature distribution indicates a realistic pathway of AW into and around the Arctic (Ilıcak et al. 2016). A more detailed evaluation of Atlantic Water core temperature (AWCT) and Atlantic Water core depth (AWCD) in simulations on this baseline grid show a temperature pattern indicating the correct circulation direction (Wang et al. 2018).

The comparison of AWI-CM1 coupled simulations to atmospheric reanalysis data and sea ice satellite observations revealed biases in the wind field over the Arctic and in the sea ice cover that were considered possible candidates for causing biases in the ocean of the coupled setup. These biases are briefly described in the following.

2.2 Coupled model bias in mean sea level pressure and sea ice

The comparison of mean sea level pressure (SLP) to the ERA5 reanalysis dataset (Hersbach et al. 2020) shows that AWI-CM1 has a bias over the central Arctic which has a dipole pattern: erroneously low SLP is found over the Canada Basin, whereas SLP is biased high over the Eurasian Basin and Barents and Kara Seas (Figure 3). The reduced pressure gradient is associated with a shift of the Beaufort High towards the Eurasian Arctic.

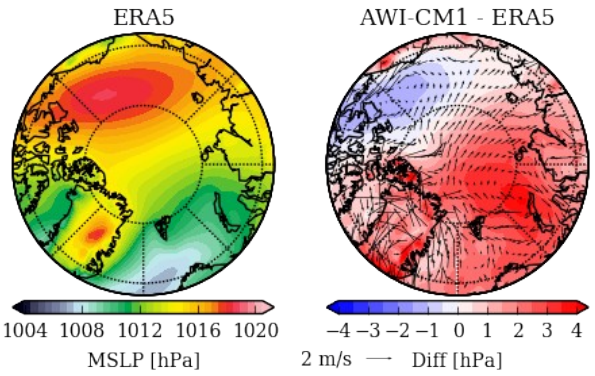

Figure 3. Mean annual sea level pressure (MSLP, [hPa]) 1980-1989 in ERA5 (left), MSLP bias [hPa] and associated wind bias in AWI-CM1 (right).

This dipole bias pattern is not unique to AWI-CM1. The coupled climate model MPI-ESM (Müller et al. 2018) which also uses ECHAM6.3 but a different ocean-sea ice model shows the same bias in pattern and magnitude (not shown). A similar SLP bias pattern also dominated the model mean of other atmospheric and coupled models not including ECHAM and it has been attributed to the truncation of the North Atlantic storm track in atmosphere models (Walsh et al. 2002).

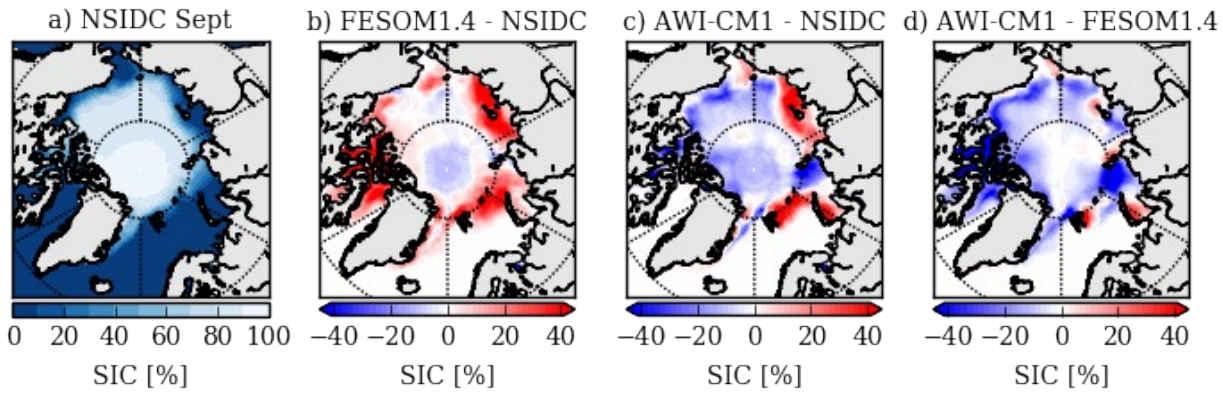

Figure 4. Mean September sea ice concentration (SIC, [%]) 1980-1989 from NSIDC (a), difference in SIC between FESOM1.4 and NSIDC (b), difference in SIC between AWI-CM1 and NSIDC (c), and difference in SIC between AWI-CM1 and FESOM1.4 (d)

The comparison of average September sea ice concentration from the coupled simulation to a standalone ocean ice model simulation and to satellite observations (NSIDC, Cavalieri (1996)) shows that AWI-CM1 generally simulates less sea ice than observed, except in some shelf regions including the north-eastern Barents Sea and the East Siberian Sea, and less sea ice than FESOM1.4 in forced (CORE-II forcing) mode (Figure 4). Underestimation of sea ice concentration in AWI-CM1 is also found in other seasons (not shown).

2.3 Sensitivity Experiments

Three sensitivity experiments have been devised to determine the impact of the wind bias and the bias in sea ice cover (separately and together) on AW circulation at depth (Table 1). A control simulation and the sensitivity experiments were started in 1958 from EN4 climatology (Good et al. 2013) and run with CORE-II forcing (Large and Yeager 2009) for 32 years until 1990. In sensitivity experiment 1 (WIND) the 6-hourly CORE-II wind forcing north of 67ºN, the Arctic Circle, was replaced with wind from an AWI-CM1 historical simulation run on the same ocean grid that also started in 1958 from EN4. The 6-hourly AWI-CM1 wind output was interpolated onto the CORE-II forcing grid. In sensitivity experiment 2 (ALBEDO), the ice and snow albedos are lowered to a degree where the sea ice cover is reduced to values similar to the ones found in the coupled simulation. In sensitivity experiment 3 (WIND+ALB) both changes were applied together.

Table 1. Overview sensitivity experiments

	CTL	**WIND**	**ALBEDO**	**WIND+ALB**
Wind Forcing	CORE2 forcing	CORE2 forcing, except wind forcing north of 67ºN replaced with wind from coupled simulation	CORE2 forcing	CORE2 forcing, except wind forcing north of 67ºN replaced with wind from coupled simulation
Albedo Parameters	default	default	reduced	reduced

In all four experiments the drag coefficients for the wind stress computation over ice and over water were adapted to follow the stress computation in the atmospheric component of AWI-CM1, ECHAM6.3, as closely as possible. The neutral drag coefficient over ice $Cd_{n,i}$ is set to 1.89e-3, the same value as in ECHAM6.3. The neutral drag coefficient over water $Cd_{n,w}$ is usually dependent on wind speed and computed using a bulk formula. In ECHAM6.3 it is computed using the Charnock equation (Charnock 1955). For our experiments using FESOM1.4 the neutral drag coefficient over water $Cd_{n,w}$ was set to be a constant value, 1.285e-3. This value represents the mean value of applying the Charnock relation to the most common wind speeds values over the Arctic, which are between 1 m/s and 8 m/s .

The results from the sensitivity experiments are described in the following section.

3 Results Sensitivity Experiments

First, the effect of exchanging the wind forcing and lowering the albedo on mean sea ice concentration in March and September is assessed (Figure. 5). In winter, replacing the wind forcing over the Arctic circle with wind from the coupled model results in increased sea ice concentration along the ice edge in the Greenland Sea and eastern Barents Sea. More spatially confined reductions in sea ice concentration can be seen in Davis Strait and in the central Barents Sea. In March, the reduced albedo has almost no effect on the sea ice extent, only on the sea ice thickness (not shown). Therefore, in March, the combined effect of a changed wind forcing and a reduced albedo is governed by the wind replacement in terms of sea ice concentration.
In September, the wind replacement leads to decreased sea ice concentration north of the Canadian Archipelago, in the Beaufort, Chukchi, East Siberian and Kara Seas and increased sea

ice concentration in the Laptev Sea, in the central Arctic along the transpolar drift route and in the northern Barents Sea and along eastern Greenland. Reduced albedo leads to a decrease in sea ice concentration everywhere. When wind replacement and albedo reduction are combined in experiment WIND+ALB, the sea ice concentration is mostly lower than in the control simulation except along the transpolar drift route and east of Svalbard, which is associated with the impact of winds. The significance of the impacts of changing winds and albedo on sea ice in other seasons lies between winter and summer.

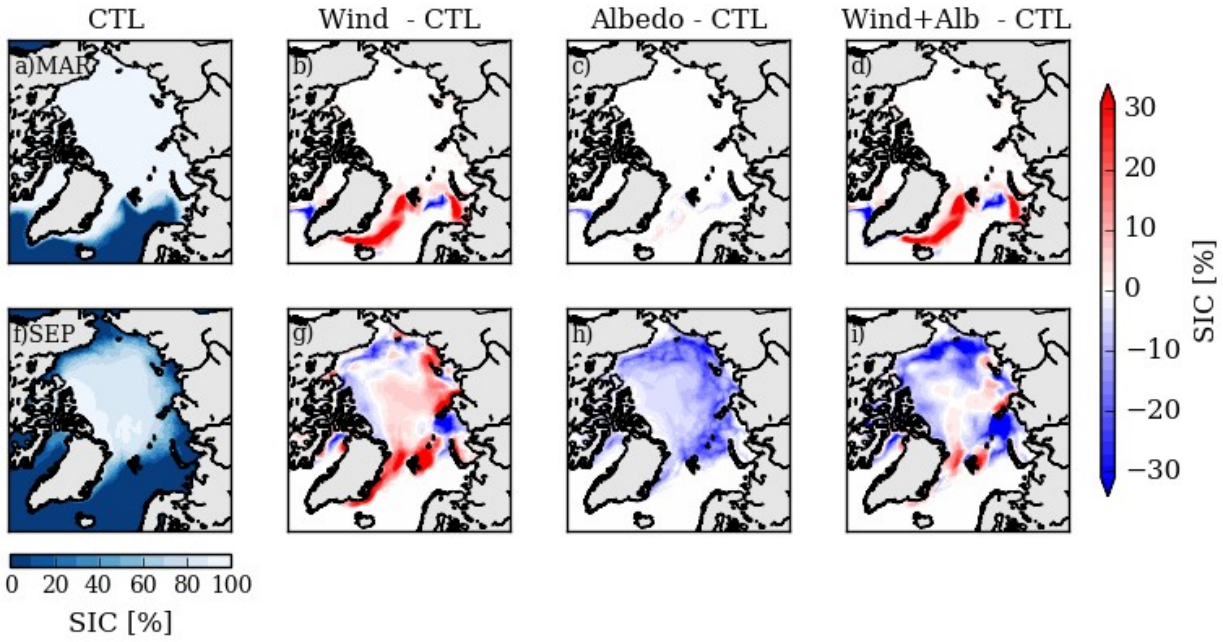

Figure 5. Differences in sea ice concentration (SIC, [%]) for March (top) and September (bottom) to control simulation

Next, the effect of the replaced wind and the albedo reduction on ocean surface conditions was investigated. The difference in surface stress between the sensitivity experiment with replaced wind forcing and the control run in the central Arctic (Figure 6a) is generally acting from the Canadian Arctic Archipelago towards the Siberian side. In the Barents Sea and the Nordic Seas, the difference in surface stress is directed westward. The surface stress difference due to reduced sea ice cover is relatively small, showing a westward component in the Eurasian Basin (Figure 6b). The differences due to the replaced wind dominate in sensitivity experiment WIND+ALB (Figure 6c).

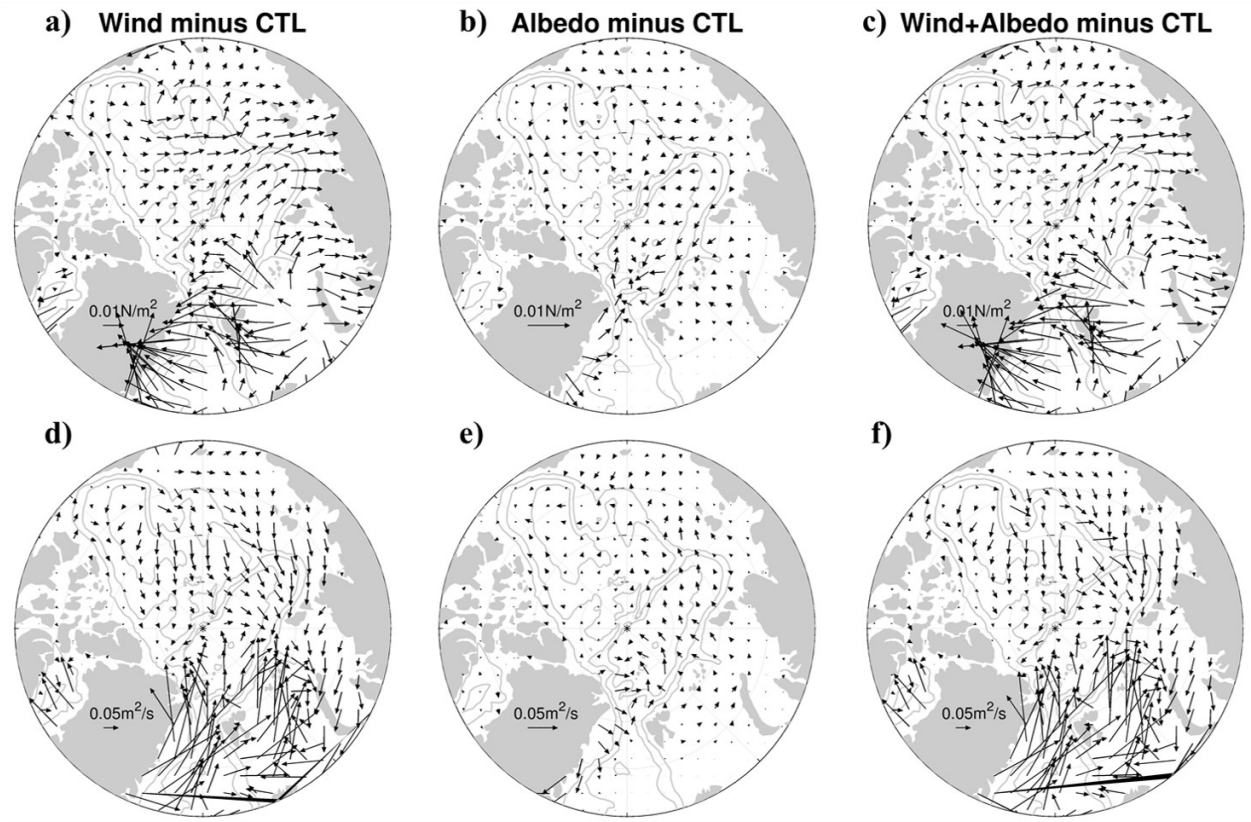

Figure 6. Ocean surface stress difference [N/m2] (a-c) and Ekman transport difference [m2/s] (d-f) for the three sensitivity experiments relative to the control run. Note that the scale for the experiment ALBEDO is doubled.

The differences in surface stress lead to differences in Ekman transport. In the experiments with replaced wind forcing the general transport pattern in the central Arctic is from the Canadian Basin towards the Eurasian side. In the Nordic Seas, the difference in Ekman transport is directed towards Fram Strait and the Barents Sea Opening and in the northern Barents Sea the difference in transport is directed towards the central Arctic (Figure 6d,f). The differences in Ekman transport in the albedo experiment are relatively small, and directed from Eurasian Basin toward the central Arctic. North of Fram Strait there is a small area with Ekman convergence (Figure 6e).

In the Arctic, the differences in Ekman transports lead to a redistribution of low salinity ocean surface water. Regions of freshwater convergence (divergence) driven by Ekman transport show an increase (decrease) in halosteric height (Figure 7a-c). Two regions with increased steric height emerge for both the wind replacement experiment and the albedo reduction experiment: In the Canadian Basin freshwater is shifted from the boundaries towards the center and in the Eurasian Basin increased heightened steric height is visible north of Fram Strait, while a decrease is visible north of the Barents and Kara Seas and in the Nordic Seas. The differences in

steric height are overall smaller for the albedo case but the effect of sea ice reduction amplifies the effect of wind perturbation in the third sensitivity experiment, where both perturbations were applied.

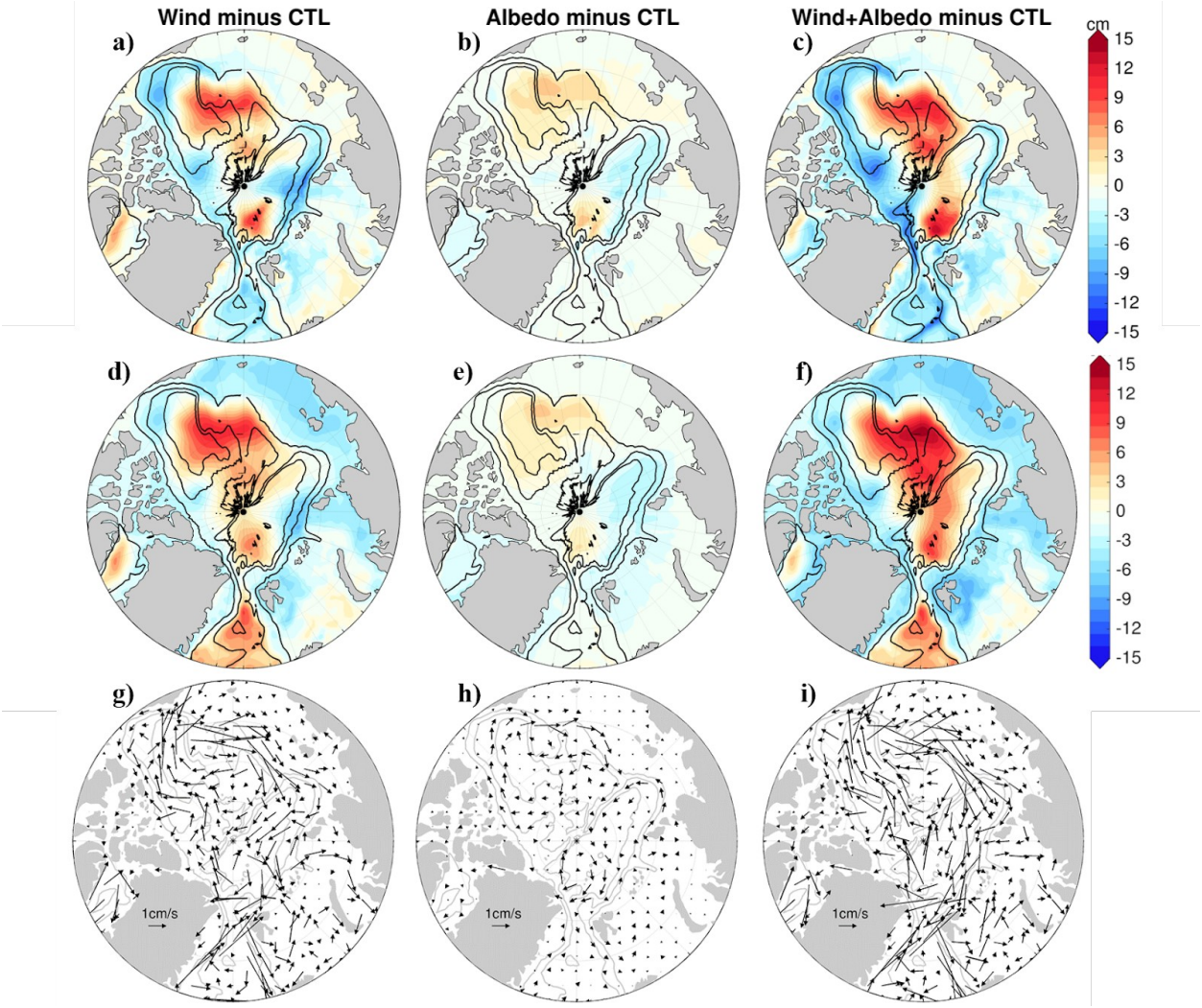

Figure 7. Halosteric height difference [cm] (a-c), sea surface height difference [cm] (d-f) and difference in geostrophic surface current velocity [cm/s] (g-i) for the three sensitivity experiments compared to the control simulation.

The differences in total sea surface height between the sensitivity runs and the control run are shown in Figure 7d-f. While these changes are driven by freshwater distribution changes in the Arctic basin, this is not the case for the Nordic Seas, where increased sea surface height in the experiments WIND and WIND+ALB cannot be explained by salinity changes and is accompanied by warmer temperatures.

The differences in sea surface height lead to differences in surface geostrophic velocity. In the WIND experiment the velocity anomaly is anticyclonic over the Arctic basin and south of

Fram Strait, in the Nordic Seas the velocity anomaly is anticyclonic as well (Figure 7g). Just north of Fram Strait the difference in geostrophic surface current points westward. In the ALBEDO experiment, there is also an anticyclonic surface geostrophic current anomaly, mostly confined to the Canadian Basin (Figure 7h). In the Eurasian Basin, there is a weak cyclonic anomaly in surface geostrophic velocity. The effect of the wind replacement is amplified again by sea ice decline in the experiment where wind and albedo are considered together (Figure 7i).

Finally, the effect of applying the wind from the coupled model and reducing sea ice cover on the horizontal temperature distribution at 400 m depth is evaluated (Figure 8). Compared to the control run, applying the wind from the coupled model leads to colder temperatures north of Fram Strait and along the cyclonic boundary current pathway. Warmer temperature can be seen along the Greenland and Canadian slope and in the Greenland Sea (Figure 8e).

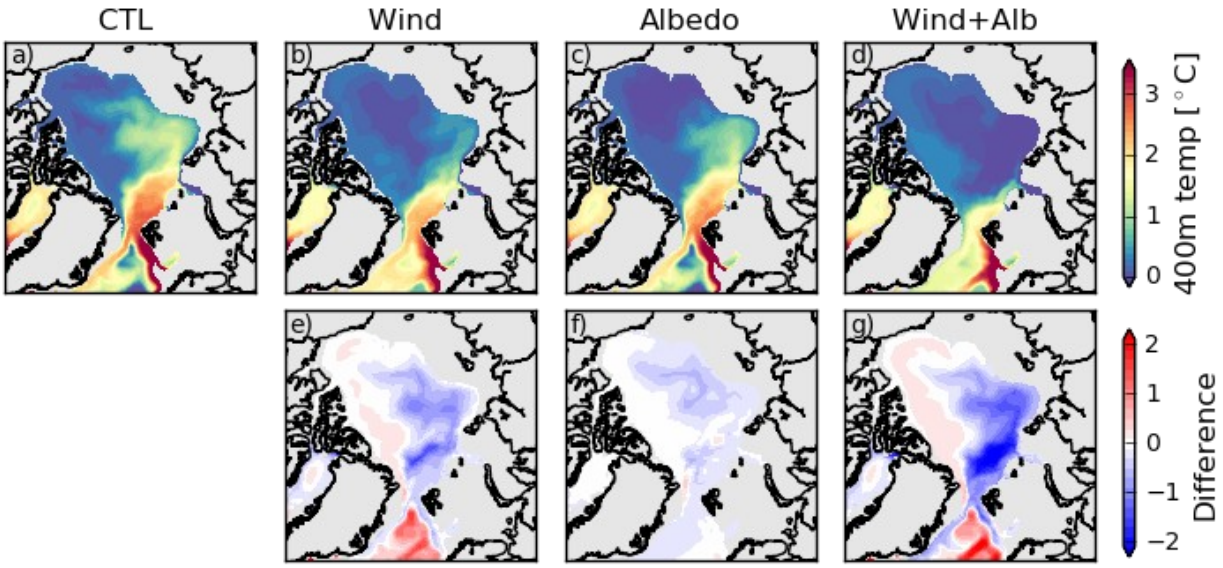

Figure 8. Mean temperature [ºC] and temperature differences to control simulation [ºC] at 400 m depth.

In experiment ALBEDO a slight cold bias has developed along the deep boundary current pathway, most pronounced at the intersection of the Eurasian Basin, the Lomonosov Ridge and the Canadian Basin, and in the Greenland Sea (Figure 8f). When wind replacement and albedo reduction are combined, the cold biases get larger (Figure 8g); in fact the warm AW is no longer visible in the boundary current beyond the Barents Sea (Figure 8d). Instead, a cold pool in the Eurasian Basin and warmer temperatures north of Greenland and Canadian Arctic Archipelago and along the southern boundary of the Canadian Basin imply a reversal of the AW flow to be anticyclonic (Figure 8d). The biased temperature distribution is remarkably similar to

the one in the coupled set-up (Figure 2b), thereby increasing confidence that biases in the coupled system can be explained by analyzing the sensitivity experiments in an ocean-only configuration.

4 Discussion

The sensitivity experiments performed with the forced ocean-sea ice model show that a bias in surface pressure and wind field over the Arctic, like the one present in AWI-CM1, together with an underestimation of the sea ice cover can result in an unrealistic temperature distribution at 400 m depth. In this case, the warm AW is no longer visible in the boundary current beyond the Barents Sea; instead a cold pool emerges in the eastern Eurasian Basin. At the same time warmer temperatures appear along the western boundary of the Arctic Ocean and in the Greenland Sea south of Fram Strait. These changes imply that part of the AW that does enter the Arctic Ocean is directed westwards and circulates the Canadian Basin anticyclonically; they also imply that less of the warm AW propagates from the Nordic Seas into the Arctic Ocean.

To investigate the former point, we computed the depth-average topostrophy between 300 m and 3,000 m. The concept of topostrophy was introduced by Holloway et al. (2007) as part of the Arctic Ocean Model Intercomparison Project (AOMIP, Proshutinsky et al. (2001)) in order to compare the simulated circulation between models. The velocity vector field is reduced to a scalar quantity τ that characterizes the tendency of a current to follow topographic slopes:

$$\tau = (V \times \nabla D) z ,$$

where **V** is velocity, D is the depth gradient, and **z** is the unit vertical vector. A positive value indicates a current with shallower water to the right (northern hemisphere) – in the case of the Arctic Circumpolar Boundary Current (ACBC) positive topostrophy indicates a cyclonic flow direction. The control simulation shows a mostly cyclonic flow all around the Arctic Ocean Basin, except for a small area north of Greenland (Figure 9a). With wind forcing from the coupled model, the circulation in the Canadian Basin turns anticyclonic (Figure 9b), most prominently on the East Siberian side. In the ALBEDO experiment the sense of the circulation over continental slopes is barely affected, only the current north of the East Siberian Sea has a slightly higher anticyclonic tendency (Figure 9c). In the experiment WIND+ALB, the circulation in most of the Canadian Basin is clearly anticyclonic, while the cyclonic circulation in the Eurasian Basin seems strengthened (Figure 9d).

In the experiments with the replaced wind forcing the mean net volume transport through the Barents Sea Opening is higher in the experiments WIND (2.4 Sv) and WIND+ALB (2.7 SV) than for CTL (2.1 Sv) and ALB (2.3 Sv). These changes are associated with the reduced SSH in the northern Barents Sea (Figure 7). The AW loses most of its heat in the Barents Sea region before entering the Arctic deep basin (Smedsrud et al. 2013) so the increased AW transport through the BSO strengthens the anticyclonic boundary circulation in the eastern Eurasian Basin (Figure 9), but it rather feeds more cold water there (Figure 8d). This effect is the most prominent in the WIND+ALB experiment which has the strongest increase in BSO inflow.

Looking at the Nordic Seas, in both simulations with replaced wind forcing the West Spitsbergen Current (WSC) and the East Greenland Current (ESC) have weakened compared to the control simulation.

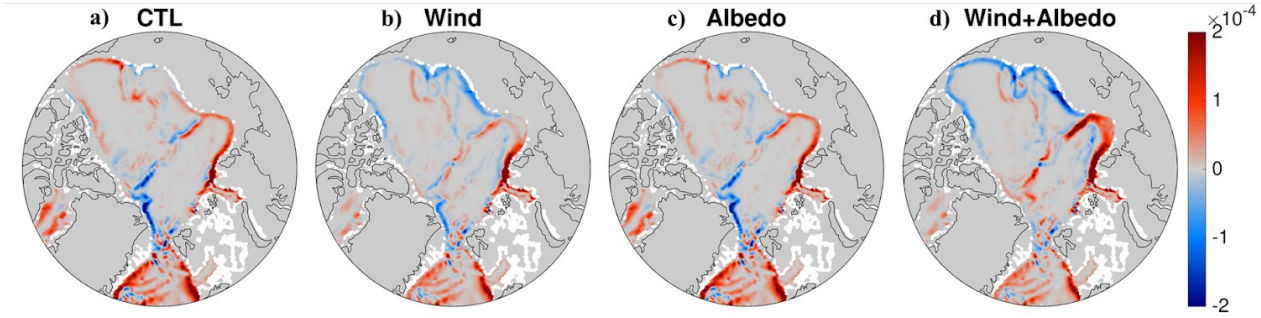

Figure 9. Mean topostrophy below 280 m depth [m^2/s] for the control simulation (CTL) and three sensitivity experiments: Wind, Albedo and Wind+Albedo.

Next, we looked at volume (not shown) and heat transports through Fram Strait at a section at 79ºN. The mean monthly net flow of heat through Fram Strait into the Arctic is higher for the control simulation (28.3 TW) and experiment ALBEDO (27.7 TW) than for the experiments WIND (20.2 TW) and WIND+ALB (19.1 TW) (Figure 10 a). Accumulated over 32 years of simulation, the net heat transport into the Arctic is 29% less in the WIND experiment and 32% less in the experiment WIND+ALB (Figure 10 c).

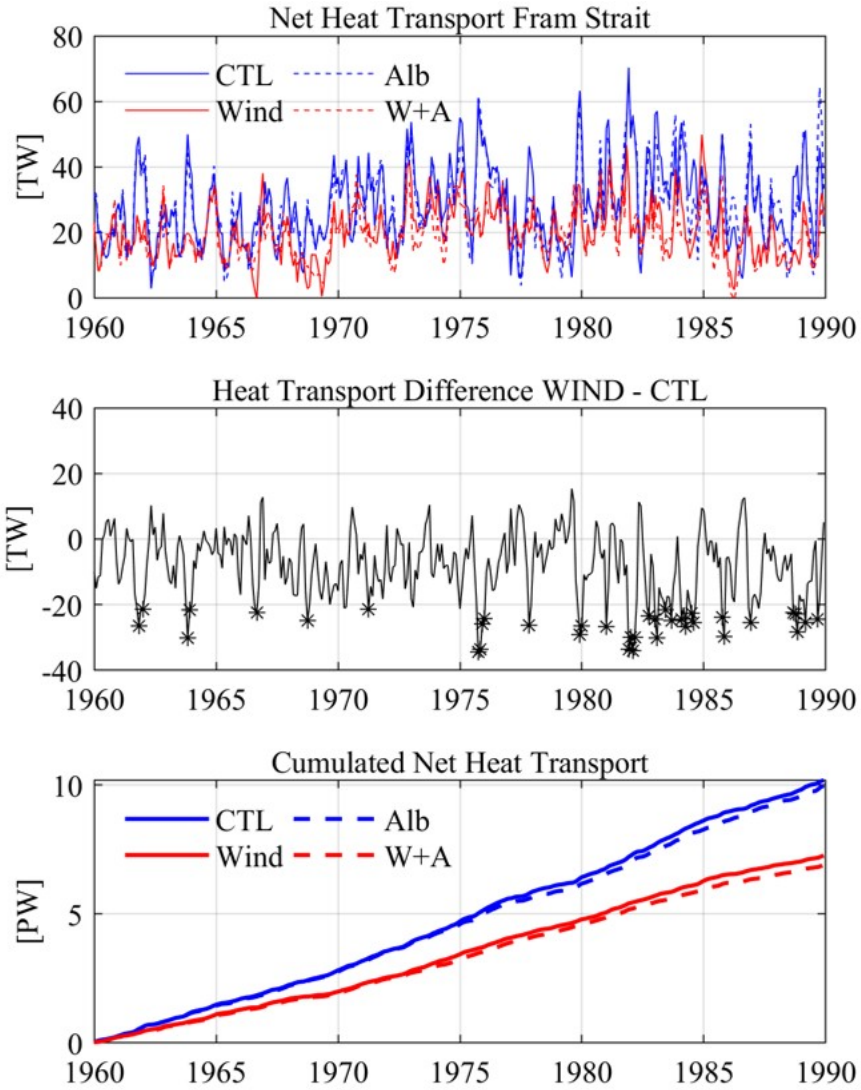

Figure 10. Time series of monthly net heat transport [TW] through Fram Strait for all experiments (a), difference [TW] between experiment 'Wind' and 'CTL'; months below 10th percentile are marked with stars (b), cumulated net heat transport [TW] for all experiments (c).

The monthly difference in net heat transport into the Arctic between experiment WIND and CTL is shown in Figure 10b. The monthly net heat transport through Fram Strait in the control simulation is larger most of the time. This can be explained by the wind bias over the Nordic Seas (Figure 11). Chatterjee et al. (2018) investigated the impact of the Greenland Sea Gyre (GSG) circulation on AW temperature variability at Fram Strait based on ocean reanalysis data and found that cold anomalies at Fram Strait are related to an atmospheric pattern that shows a high pressure anomaly centered over Svalbard, northerly winds over the western Greenland Sea and southerly wind along the Norwegian coast (Chatterjee et al. 2018, see their

figure 3c). Such a wind pattern, which resembles the model bias in AWI-CM1, leads to Ekman convergence in the GSG and positive sea surface height anomalies which weaken the cyclonic GSG circulation. Figure 7d shows the difference in SSH between the 'Wind' experiment and the control run with a positive height difference in the Nordicd Seas. A composite of sea surface height differences in the months with the largest negative net heat transport differences (Figure 10b, starred months show 10th percentile) shows even higher SSH differences (not shown). The increased SSH in the Nordic Seas reduces AW transport to the Nordic Seas across Iceland-Scotland Ridge (not shown). Therefore, the wind anomaly both reduces AW transport toward the Arctic Ocean and increases the amount of AW leaving through the BSO. The consequence is the reduction in the AW transport in the West Spitsbergen Current at Fram Strait and in the AW recirculation in the EGC.

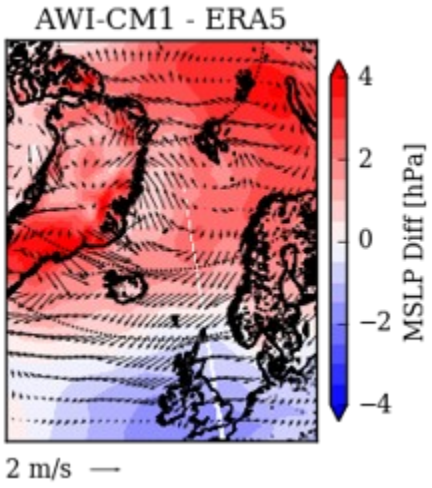

Figure 11. AWI-CM1 MSLP [hPa] and wind bias compared to ERA5 with focus on the Nordic Seas

Because we set out to understand the influence of large-scale wind biases in a coupled model, we did not separate the wind bias into a local (over the central Arctic) and remote (over the Nordic Seas) component for the sensitivity experiments. Nonetheless, the results discussed above are consistent with previous model studies on the role of local and remote wind forcing for the ACBC: Lique et al. (2015) and Lique and Johnson (2015) studied the influence of local and remote wind forcing on the AW circulation at depth. They found that remote wind forcing over the Nordic and Barents Seas can drive a direct and fast response of the AW circulation in the Arctic Ocean through a change of AW inflow, while the local wind forcing of the Canadian

Basin results in slower changes 'filtered' by the surface circulation which in turn modulates the deeper AW circulation. Here, a stronger anticyclonic wind forces a strong, deep Beaufort Gyre in the same direction, so that no deep counterflow can develop.

Although the bias in sea ice cover does not affect net heat transports through Fram Strait (Figure 10c), the sensitivity experiment with reduced albedo shows that a reduced sea ice cover does influence the distribution of freshwater at the surface (Figure 7b). Its effect on the ocean surface is smaller compared to the wind bias but it also leads to a strengthening of the anticyclonic surface current in the western Arctic (Figure 7h). This effect of sea ice decline on the surface dynamics of the Arctic Ocean was also shown by Wang et al. (2019). (2019). Earlier, Spall (2013) had shown, based on idealized model simulations, that when the ice-ocean stress was removed completely, the anticyclonic circulation in the western basin is lost and eddy fluxes from the boundary are enhanced, indicating that the instability of the boundary current is suppressed by ice cover. Ideally, this potential consequence of sea ice decline and related feedback should be further investigated with skillful coupled models projecting future Arctic conditions.

This study has investigated the influence of a SLP and wind bias specific to the coupled climate model AWI-CM1. It is worth stressing that this bias is not unique to AWI-CM1 – another CMIP6 model, MPI-ESM, that also employs ECHAM6.3 as its atmosphere component but has a different ocean-sea ice component, shows a nearly identical SLP bias, both in shape and magnitude. Furthermore, it has been found in other atmospheric models as well and it is the prominent feature in multi-model-means of SLP bias in model intercomparison studies of coupled and uncoupled models (Walsh et al. 2002). The truncation of the North Atlantic storm track, which prevents Atlantic cyclones from moving further north into the Norwegian, Barents and Kara Seas region in the models, has been suggested as a cause for this bias. It has also been suggested that biased surface winds in the Arctic can adversely affect sea ice transport and the resulting distribution of sea ice concentration and thickness, as well as the export of ice and freshwater to the North Atlantic (Walsh et al. 2002; Chapman and Walsh 2007). Our study shows that this wind bias pattern can additionally affect the simulated circulation in the deep Arctic Ocean by imposing an anticyclonic surface circulation anomaly which in turn imprints on

the deeper ocean circulation. Our results also reveal that a negative sea ice bias could amplify this issue.

Walsh et al. (2002) recommended that efforts to ameliorate the SLP bias in atmospheric models should be focused on the representation of topography over northern Asia and Greenland and specifically topographic parameterizations which could affect the exchange of mass between Asia and the Arctic Ocean. They note that the resolution of the atmosphere model may also play a role for the magnitude of the bias. For AWI-CM1, we tried tuning some parameters related to model topography (gk_wake, gk_drag and gk_lift) without being able to significantly reduce the SLP bias or the circulation bias (not shown).

Mu et al. (2020) showed that the assimilation of sea surface temperature into AWI-CM1 leads to a more realistic atmospheric circulation and did reverse the erroneous direction of the deep boundary current carrying AW after 8 simulation years with data assimilation. This reversal of the current to a cyclonic flow is attributed to the improvement of atmosphere states over the ice-free area that can further propagate to the whole Arctic dynamically.

5 Conclusions

Atlantification might be an important driver in amplified Arctic sea ice melting and warming (Årthun et al. 2019) and regional differences in sea ice loss (Årthun et al. 2021). In order to study the evolution of Atlantification and the associated feedback in the Arctic climate system with global coupled climate models, the AW inflow and Arctic Ocean circulation need to be simulated realistically. A skill assessment of the AW layer representation in CMIP5 (Shu et al. 2019) and CMIP6 (Khosravi et al., submitted) models show that in many of the models that do simulate a distinct Arctic AW layer, this layer is too thick, too deep or does not show the observed warming trend. These types of biases are commonly related to insufficient resolution and too much mixing in the ocean component as well as unrealistic Atlantik-Arctic Ocean exchange.

Our study shows that even if all impediments for simulating AW realistically are addressed in the ocean model, e.g. sufficient resolution in the horizontal and vertical, Arctic gateways-resolving grid resolution and bathymetry, the right amount of mixing, etc., new obstacles may arise after coupling to an atmosphere model with its own shortcomings in the Arctic. AWI-CM1, like many other coupled climate models, has a bias in SLP over the Arctic Ocean with higher

458 pressure over the Eurasian Basin and Barents and Kara Seas and lower SLP over the Canada
459 Basin. In the Arctic Ocean, the bias in wind stress related to the biased surface pressure gradient
460 leads to differences in Ekman transport, freshwater distribution and steric height that strengthens
461 the anticyclonic surface circulation in the Canadian Basin, so that the deep counterflow gets
462 reversed. This effect is visualized by negative topostrophy (Figure 9b,d) and the warm bias
463 (Figure 8e,g) in the Canada Basin. An underestimation of sea ice concentration as seen in AWI-
464 CM1 can amplify the described processes locally. In the Nordic Seas, an anticyclonic wind bias
465 increases the sea surface height and weakens the cyclonic gyre circulation there, which leads to
466 reduced volume and heat (proxy for AW) transport into the Arctic Ocean through Fram Strait. At
467 the same time, the wind bias also increases AW transport through the BSO, which feeds cold
468 water to the deep basin.The overall effect is a cold bias in the Eurasin Basin (Figure 8e,g).
469 The problem of biased SLP over the Arctic cannot be overcome easily. Efforts to tune
470 parameters related to model topography as suggested by Walsh et al. (2002) did not lead to a
471 significant reduction of the SLP bias or the circulation bias in our practice. SST assimilation
472 seems to rectify the circulation in AWI-CM1, but this constraint cannot be applied to the future
473 scenario simulations of course.
474 Currently, a new version 3 of AWI-CM is in development. In this version, ECHAM is
475 replaced with open IFS (OFIS, Roberts et al. (2018)) for the atmosphere component. Preliminary
476 results show that the SLP bias over the Arctic is also present in OIFS but it is of smaller
477 magnitude than in ECHAM. The temperature distribution at 400 m implies a cyclonic
478 circumpolar circulation in simulations with AWI-CM3. This new model version is not released
479 yet, and will be described later separately after the initial model tuning process is finished.
480 The Arctic is a hotspot in global warming, but there is still a large inter-model spread and
481 model uncertainty in CMIP6 projections of the surface warming - especially in the Arctic (Cai et
482 al. 2021). Detailed investigations of model biases are needed to improve the simulations and
483 reduce sources of model uncertainty. Simulating ocean heat transport into and within the Arctic
484 more faithfully will help to understand and predict future Arctic changes better.

485 **Acknowledgments and Data Availability**

486 C. Hinrichs, T. Semmler, and T. Jung have received funding from the European Union's
487 Horizon 2020 Research and Innovation program through grant agreement No. 727862

APPLICATE. This is a contribution to the Year of Polar Prediction (YOPP), a flagship activity of the Polar Prediction Project (PPP), initiated by the World Weather Research Programme (WWRP) of the World Meteorological Organisation (WMO). We acknowledge the WMO WWRP for its role in coordinating this international research activity. The work described in this paper has also received funding from the Helmholtz Association through the project 'Regional Climate Change (REKLIM)' and "Advanced Earth System Model Capacity". The simulations were performed at the German Climate Computing Center (DKRZ) using ESM-Tools (https://www.esm-tools.net/).

Our model simulations were compared to the Polar science center Hydrographic Climatology (PHC) version 3.0 (available at http://psc.apl.washington.edu/nonwp_projects/PHC/Climatology.html), to ERA5 reanalysis data (downloaded from the Copernicus data store at https://cds.climate.copernicus.eu/cdsapp#!/home), and sea ice concentration data from the National Snow & Ice Data Center (https://nsidc.org/).

Data from the sensitivity experiments will be made available at https://zenodo.org/ for before final submission.

References

Aagaard, K. 1989. *A synthesis of the Arctic Ocean circulation*. Le Conseil.

Årthun, M., T. Eldevik, and L.H. Smedsrud. 2019. The role of Atlantic heat transport in future Arctic winter sea ice loss. *Journal of Climate* 32: 3327-3341.

Årthun, M., I.H. Onarheim, J. Dörr, and T. Eldevik. 2021. The Seasonal and Regional Transition to an Ice-Free Arctic. *Geophysical Research Letters* 48: e2020GL090825.

Barton, B.I., Y.-D. Lenn, and C. Lique. 2018. Observed Atlantification of the Barents Sea causes the polar front to limit the expansion of winter sea ice. *Journal of Physical Oceanography* 48: 1849-1866.

Beszczynska-Möller, A., E. Fahrbach, U. Schauer, and E. Hansen. 2012. Variability in Atlantic water temperature and transport at the entrance to the Arctic Ocean, 1997–2010. *ICES Journal of Marine Science* 69: 852-863.

Cai, Z., Q. You, F. Wu, H.W. Chen, D. Chen, and J. Cohen. 2021. Arctic warming revealed by multiple CMIP6 models: evaluation of historical simulations and quantification of future projection uncertainties. *Journal of Climate*: 1-52.

Cavalieri, D.J., C. L. Parkinson, P. Gloersen, and H. J. Zwally. 1996. Sea Ice Concentrations from Nimbus-7 SMMR and DMSP SSM/I-SSMIS Passive Microwave Data, Version 1., ed. Colorado USA. NASA National Snow and Ice Data Center Distributed Active Archive Center. Boulder.

Chapman, W.L., and J.E. Walsh. 2007. Simulations of Arctic temperature and pressure by global coupled models. *Journal of Climate* 20: 609-632.

Charnock, H. 1955. Wind stress on a water surface. *Quarterly Journal of the Royal Meteorological Society* 81: 639-640.

Chatterjee, S., R.P. Raj, L. Bertino, Ø. Skagseth, M. Ravichandran, and O.M. Johannessen. 2018. Role of Greenland Sea Gyre Circulation on Atlantic Water Temperature Variability in the Fram Strait. *Geophysical Research Letters* 0.

Cohen, J., X. Zhang, J. Francis, T. Jung, R. Kwok, J. Overland, T. Ballinger, U. Bhatt, H. Chen, and D. Coumou. 2020. Divergent consensuses on Arctic amplification influence on midlatitude severe winter weather. *Nature Climate Change* 10: 20-29.

Danilov, S., Q. Wang, R. Timmermann, N. Iakovlev, D. Sidorenko, M. Kimmritz, T. Jung, and J. Schröter. 2015. Finite-Element Sea Ice Model (FESIM), version 2. *Geosci. Model Dev.* 8: 1747-1761.

Dmitrenko, I.A., I.V. Polyakov, S.A. Kirillov, L.A. Timokhov, I.E. Frolov, V.T. Sokolov, H.L. Simmons, V.V. Ivanov, and D. Walsh. 2008. Toward a warmer Arctic Ocean: Spreading of the early 21st century Atlantic Water warm anomaly along the Eurasian Basin margins. *Journal of Geophysical Research: Oceans* 113.

Golubeva, E., and G. Platov. 2007. On improving the simulation of Atlantic Water circulation in the Arctic Ocean. *Journal of Geophysical Research: Oceans* 112.

Good, S.A., M.J. Martin, and N.A. Rayner. 2013. EN4: Quality controlled ocean temperature and salinity profiles and monthly objective analyses with uncertainty estimates. *Journal of Geophysical Research: Oceans* 118: 6704-6716.

Griffies, S.M., A. Biastoch, C. Böning, F. Bryan, G. Danabasoglu, E.P. Chassignet, M.H. England et al. 2009. Coordinated Ocean-ice Reference Experiments (COREs). *Ocean Modelling* 26: 1-46.

Holloway, G., F. Dupont, E. Golubeva, S. Häkkinen, E. Hunke, M. Jin, M. Karcher, F. Kauker, M. Maltrud, and M.M. Maqueda. 2007. Water properties and circulation in Arctic Ocean models. *Journal of Geophysical Research: Oceans* 112.

Holloway, G., and Z. Wang. 2009. Representing eddy stress in an Arctic Ocean model. *Journal of Geophysical Research: Oceans* 114.

Ilıcak, M., H. Drange, Q. Wang, R. Gerdes, Y. Aksenov, D. Bailey, M. Bentsen et al. 2016. An assessment of the Arctic Ocean in a suite of interannual CORE-II simulations. Part III: Hydrography and fluxes. *Ocean Modelling* 100: 141-161.

Itkin, P., M. Karcher, and R. Gerdes. 2014. Is weaker Arctic sea ice changing the Atlantic water circulation? *Journal of Geophysical Research: Oceans* 119: 5992-6009.

Ivanov, V., A. Smirnov, V. Alexeev, N.V. Koldunov, I. Repina, and V. Semenov. 2018. Contribution of Convection−Induced Heat Flux to Winter Ice Decay in the Western Nansen Basin. *Journal of Geophysical Research: Oceans* 123: 6581-6597.

Jung, T., N.D. Gordon, P. Bauer, D.H. Bromwich, M. Chevallier, J.J. Day, J. Dawson, F. Doblas-Reyes, C. Fairall, and H.F. Goessling. 2016. Advancing polar prediction capabilities on daily to seasonal time scales. *Bulletin of the American Meteorological Society* 97: 1631-1647.

Karcher, M., F. Kauker, R. Gerdes, E. Hunke, and J. Zhang. 2007. On the dynamics of Atlantic Water circulation in the Arctic Ocean. *Journal of Geophysical Research: Oceans* 112.

Khosravi, N., Q. Wang, N. Koldunov, C. Hinrichs, T. Semmler, S. Danilov, and T. Jung. Arctic Ocean in CMIP6 Models: Historical and projected temperature and salinity in the deep basins. *Earth's Future*. Preprint available at https://www.essoar.org/doi/abs/10.1002/essoar.10505254.1.

Koenigk, T., and L. Brodeau. 2014. Ocean heat transport into the Arctic in the twentieth and twenty-first century in EC-Earth. *Climate Dynamics* 42: 3101-3120.

Koldunov, N.V., V. Aizinger, N. Rakowsky, P. Scholz, D. Sidorenko, S. Danilov, and T. Jung. 2019. Scalability and some optimization of the Finite-volumE Sea ice–Ocean Model, Version 2.0 (FESOM2). *Geoscientific Model Development* 12: 3991-4012.

Large, W.G., and S. Yeager. 2009. The global climatology of an interannually varying air–sea flux data set. *Climate Dynamics* 33: 341-364.

Lique, C., and H.L. Johnson. 2015. Is there any imprint of the wind variability on the Atlantic Water circulation within the Arctic Basin? *Geophysical Research Letters* 42: 9880-9888.

Lique, C., H.L. Johnson, and P.E.D. Davis. 2015. On the Interplay between the Circulation in the Surface and the Intermediate Layers of the Arctic Ocean. *Journal of Physical Oceanography* 45: 1393-1409.

Maqueda, M.M., and G. Holloway. 2006. Second-order moment advection scheme applied to Arctic Ocean simulation. *Ocean Modelling* 14: 197-221.

Mu, L., L. Nerger, Q. Tang, S.N. Loza, D. Sidorenko, Q. Wang, T. Semmler, L. Zampieri, M. Losch, and H.F. Goessling. 2020. Toward a data assimilation system for seamless sea ice prediction based on the AWI climate model. *Journal of Advances in Modeling Earth Systems* 12: e2019MS001937.

Müller, W.A., J.H. Jungclaus, T. Mauritsen, J. Baehr, M. Bittner, R. Budich, F. Bunzel, M. Esch, R. Ghosh, and H. Haak. 2018. A Higher−resolution Version of the Max Planck Institute Earth System Model (MPI−ESM1. 2−HR). *Journal of Advances in Modeling Earth Systems* 10: 1383-1413.

Nazarenko, L., G. Holloway, and N. Tausnev. 1998. Dynamics of transport of "Atlantic signature" in the Arctic Ocean. *Journal of Geophysical Research: Oceans* 103: 31003-31015.

Polyakov, I.V., A. Beszczynska, E.C. Carmack, I.A. Dmitrenko, E. Fahrbach, I.E. Frolov, R. Gerdes, E. Hansen, J. Holfort, and V.V. Ivanov. 2005. One more step toward a warmer Arctic. *Geophysical Research Letters* 32.

Polyakov, I.V., U.S. Bhatt, J.E. Walsh, E.P. Abrahamsen, A.V. Pnyushkov, and P.F. Wassmann. 2013. Recent oceanic changes in the Arctic in the context of long−term observations. *Ecological Applications* 23: 1745-1764.

Polyakov, I.V., A.V. Pnyushkov, M.B. Alkire, I.M. Ashik, T.M. Baumann, E.C. Carmack, I. Goszczko, J. Guthrie, V.V. Ivanov, and T. Kanzow. 2017. Greater role for Atlantic inflows on sea-ice loss in the Eurasian Basin of the Arctic Ocean. *Science* 356: 285-291.

Polyakov, I.V., T.P. Rippeth, I. Fer, M.B. Alkire, T.M. Baumann, E.C. Carmack, R. Ingvaldsen et al. 2020. Weakening of Cold Halocline Layer Exposes Sea Ice to Oceanic Heat in the Eastern Arctic Ocean. *Journal of Climate* 33: 8107-8123.

Proshutinsky, A., M. Steele, J. Zhang, G. Holloway, N. Steiner, S. Häkkinen, D. Holland, R. Gerdes, C. Köberle, and M. Karcher. 2001. The Arctic Ocean Model Intercomparison Project (AOMIP). *Eos Trans. AGU* 82: 637-644.

Rackow, T., H.F. Goessling, T. Jung, D. Sidorenko, T. Semmler, D. Barbi, and D. Handorf. 2016. Towards multi-resolution global climate modeling with ECHAM6-FESOM. Part II: climate variability. *Climate Dynamics*: 1-26.

Roberts, C.D., R. Senan, F. Molteni, S. Boussetta, M. Mayer, and S.P. Keeley. 2018. Climate model configurations of the ECMWF Integrated Forecasting System (ECMWF-IFS cycle 43r1) for HighResMIP. *Geoscientific Model Development* 11: 3681-3712.

Rudels, B., H.J. Friedrich, and D. Quadfasel. 1999. The Arctic circumpolar boundary current. *Deep Sea Research Part II: Topical Studies in Oceanography* 46: 1023-1062.

Semmler, T., S. Danilov, P. Gierz, H.F. Goessling, J. Hegewald, C. Hinrichs, N. Koldunov et al. 2020. Simulations for CMIP6 With the AWI Climate Model AWI-CM-1-1. *Journal of Advances in Modeling Earth Systems* 12: e2019MS002009.

Serreze, M., A. Barrett, J. Stroeve, D. Kindig, and M. Holland. 2009. The emergence of surface-based Arctic amplification. *The Cryosphere* 3: 11.

Serreze, M.C., and R.G. Barry. 2011. Processes and impacts of Arctic amplification: A research synthesis. *Global and planetary change* 77: 85-96.

Shu, Q., Q. Wang, J. Su, X. Li, and F. Qiao. 2019. Assessment of the Atlantic water layer in the Arctic Ocean in CMIP5 climate models. *Climate Dynamics* 53: 5279-5291.

Sidorenko, D., T. Rackow, T. Jung, T. Semmler, D. Barbi, S. Danilov, K. Dethloff, W. Dorn, K. Fieg, and H.F. Gößling. 2015. Towards multi-resolution global climate modeling with ECHAM6–FESOM. Part I: model formulation and mean climate. *Climate Dynamics* 44: 757-780.

Smedsrud, L.H., I. Esau, R.B. Ingvaldsen, T. Eldevik, P.M. Haugan, C. Li, V.S. Lien, A. Olsen, A.M. Omar, and O.H. Otterå. 2013. The role of the Barents Sea in the Arctic climate system. *Reviews of Geophysics* 51: 415-449.

Spall, M.A. 2013. On the Circulation of Atlantic Water in the Arctic Ocean. *Journal of Physical Oceanography* 43: 2352-2371.

Steele, M., R. Morley, and W. Ermold. 2001. PHC: A global ocean hydrography with a high-quality Arctic Ocean. *Journal of Climate* 14: 2079-2087.

Stevens, B., M. Giorgetta, M. Esch, T. Mauritsen, T. Crueger, S. Rast, M. Salzmann, H. Schmidt, J. Bader, and K. Block. 2013. Atmospheric component of the MPI−M Earth System Model: ECHAM6. *Journal of Advances in Modeling Earth Systems* 5: 146-172.

629 Timmermans, M.-L., and J. Marshall. 2020. Understanding Arctic Ocean Circulation: A Review of Ocean Dynamics
630 in a Changing Climate. *Journal of Geophysical Research: Oceans* 125: e2018JC014378.
631 Vihma, T. 2014. Effects of Arctic Sea Ice Decline on Weather and Climate: A Review. *Surveys in Geophysics* 35:
632 1175-1214.
633 Wallace, J.M., I.M. Held, D.W. Thompson, K.E. Trenberth, and J.E. Walsh. 2014. Global warming and winter
634 weather. *Science* 343: 729-730.
635 Walsh, J.E., V.M. Kattsov, W.L. Chapman, V. Govorkova, and T. Pavlova. 2002. Comparison of Arctic climate
636 simulations by uncoupled and coupled global models. *Journal of Climate* 15: 1429-1446.
637 Wang, Q., S. Danilov, D. Sidorenko, R. Timmermann, C. Wekerle, X. Wang, T. Jung, and J. Schröter. 2014. The
638 Finite Element Sea Ice-Ocean Model (FESOM) v. 1.4: formulation of an ocean general circulation model.
639 *Geoscientific Model Development* 7: 663-693.
640 Wang, Q., M. Ilicak, R. Gerdes, H. Drange, Y. Aksenov, D.A. Bailey, M. Bentsen et al. 2016a. An assessment of the
641 Arctic Ocean in a suite of interannual CORE-II simulations. Part I: Sea ice and solid freshwater. *Ocean*
642 *Modelling* 99: 110-132.
643 Wang, Q., M. Ilicak, R. Gerdes, H. Drange, Y. Aksenov, D.A. Bailey, M. Bentsen et al. 2016b. An assessment of
644 the Arctic Ocean in a suite of interannual CORE-II simulations. Part II: Liquid freshwater. *Ocean*
645 *Modelling* 99: 86-109.
646 Wang, Q., C. Wekerle, S. Danilov, D. Sidorenko, N. Koldunov, D. Sein, B. Rabe, and T. Jung. 2019. Recent Sea Ice
647 Decline Did Not Significantly Increase the Total Liquid Freshwater Content of the Arctic Ocean. *Journal*
648 *of Climate* 32: 15-32.
649 Wang, Q., C. Wekerle, S. Danilov, X. Wang, and T. Jung. 2018. A 4.5 km resolution Arctic Ocean simulation with
650 the global multi-resolution model FESOM 1.4. *Geoscientific Model Development* 11: 1229.
651 Wang, Q., C. Wekerle, X. Wang, S. Danilov, N. Koldunov, D. Sein, D. Sidorenko, W.J. von Appen, and T. Jung.
652 2020. Intensification of the Atlantic Water supply to the Arctic Ocean through Fram Strait induced by
653 Arctic sea ice decline. *Geophysical Research Letters* 47: e2019GL086682.
654 Woodgate, R.A., K. Aagaard, R.D. Muench, J. Gunn, G. Björk, B. Rudels, A. Roach, and U. Schauer. 2001. The
655 Arctic Ocean boundary current along the Eurasian slope and the adjacent Lomonosov Ridge: Water mass
656 properties, transports and transformations from moored instruments. *Deep Sea Research Part I:*
657 *Oceanographic Research Papers* 48: 1757-1792.
658 Zhang, J., and M. Steele. 2007. Effect of vertical mixing on the Atlantic Water layer circulation in the Arctic Ocean.
659 *Journal of Geophysical Research: Oceans* 112.